Hindawi
International Journal of Geophysics
Volume 2018, Article ID 1298087, 13 pages
https://doi.org/10.1155/2018/1298087

Research Article

Depth and Lineament Maps Derived from North Cameroon Gravity Data Computed by Artificial Neural Network

Marcelin Mouzong Pemi,[1,2] **Joseph Kamguia**,[3] **Severin Nguiya**,[4] **and Eliezer Manguelle-Dicoum**[1]

[1]*Faculty of Science, University of Yaounde 1, P.O. Box 812, Yaounde, Cameroon*
[2]*Department of Renewable Energy, Higher Technical Teachers' Training College (HTTTC), University of Buea, P.O. Box 249, Cameroon*
[3]*National Institute of Cartography (NIC), P.O. Box 157, Yaounde, Cameroon*
[4]*Faculty of Industrial Engineering, University of Douala, P.O. Box 2701, Cameroon*

Correspondence should be addressed to Marcelin Mouzong Pemi; mouzong.pemi@ubuea.cm

Received 3 January 2018; Revised 15 April 2018; Accepted 12 May 2018; Published 5 July 2018

Academic Editor: Filippos Vallianatos

Accurate interpretation of geological structures inverted from gravity data is highly dependent on the coverage of the recorded gravity data. In this work, Artificial Neural Networks (ANNs) are implemented using Levenberg-Marquardt algorithm (LMA) to construct a background density model for predicting gravity data across Northern Cameroon and its surroundings. This approach yields statistical predictions of gravity values (low values of errors) with 97.48%, 0.10, and 0.89, respectively, for correlation, Mean Bias Error, and Root Mean Square Error for two inputs (latitude, longitude) and 97.08%, 0.13, and 1.14 for three inputs (latitude, longitude, and elevation) for a set of anomalies as output. The model validation is obtained by comparing the results to other classical approaches and to the computed Bouguer, lineaments, and Euler maps obtained from measured gravity data. The depth of most of the deep faults and their orientation are in agreement with those obtained from other studies. The results achieved in this study establish the possibility of enhancing the quality of the analysis, interpretation, and modeling of gravity data collected on sparse grid of recording stations.

1. Introduction

The Northern Cameroon and its surroundings, the subject of this study, have prompted many researchers and prospectors to identify superficial and deep structures and to indicate their geodynamics and tectonic implications [1–5]. The vast majority of these studies used the data from surveys carried out by French Research Institute for Development (IRD) and other private and public institutions. Unfortunately, these data are scattered and unevenly distributed over the Cameroonian territory since they were mostly collected along available roads. Researchers have used interpolation techniques to extract relevant information from uncovered areas, such as Generic Mapping Tool (GMT) [6], minimum curvature [7], kriging [8, 9], the least-squares method [10], and finite element approach through cubic B-spline function [11]. These methods have yielded interesting results and allowed in specific cases extracting relevant information from uncovered areas. However, the reliability and robustness of these conventional interpolation techniques are hampered by a limited number of input variables and a small sample size. These limit the validity of the reconstructed density models to narrow areas. In order to construct models that cover large areas more robustly, we propose to use ANN technique through Levenberg-Marquardt algorithm.

Haykin [12] defined Neural Network as a massively parallel distributed processor made up of simple processing units that has a natural propensity for storing experiential knowledge and making it available for use like the brain. They have recently gained in popularity in geophysics and have been applied to a variety of problems. Geophysical problems such as seismic waveform recognition [13], first-break picking

Figure 1: Spatial distribution in the study area.

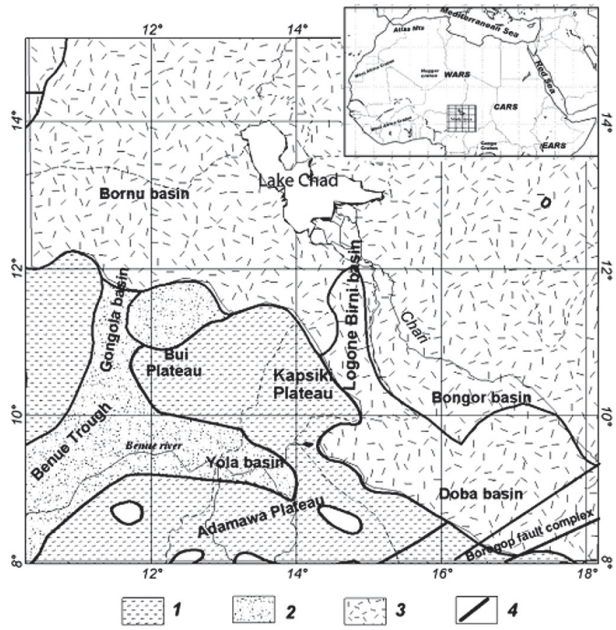

Figure 2: Geological map of the study area: (1) Precambrian; (2) Early Cretaceous; (3) Tertiary-Quaternary; and (4) faults or major structural elements (modified from Eyike et al., 2010).

and trace editing [14], earthquake prediction [15, 16], electromagnetic [17], magnetotelluric [18], seismic inversion [19–21], shear-wave splitting [22], well-log analysis [23], seismic deconvolution [24, 25], seismic discrimination [26], and seismic signals detection and classification [27] used ANNs to forecast the unknown. Grêt et al. [28] and Ghalambaz et al. [29] performed gravity interpretations in two dimensions and event classification, respectively, to discriminate bodies of a similar kind of anomaly and approximate shape parameters like depth, vertical extension, and radius. They use a Hybrid Neural Network and Gravitational Search Algorithm (HNGSA) to solve Wessinger's equation [29]. In this paper, we develop a background density model using ANN to extract gravity anomalies with their geographical variables (latitude, longitude, and elevation). The model integrates input and output data of an area covering North Cameroon and its surroundings (Figure 1) measured by IRD. In addition, a model validation is carried out by establishing Bouguer and residual maps of the studied area and then comparing them to those obtained by ANN. With this approach, we expect the estimation of gravity values in uncovered areas during data acquisition. The results show that ANNs can be used to interpolate data of uncovered area and increase the resolution of geological structures in poorly covered areas.

2. Geology of the Area

The data used in this study cover three main domains: northern extension of Benue trough in the East of Nigeria, Northern Cameroon, and West of Chad (Doba basin). Fairhead and Okereke [30] listed four important events in West Central Africa Rift System: extensional, compressional, tectonics, and subsidence. The surface geology (Figure 2) is mainly composed of the Precambrian basement made up of migmatites and anatectites of the Mokolo unit [31] and formations of the Pan African Mobile Belt. Old sediments (Early Cretaceous in age) of 4 km thickness cover the Garoua sedimentary basin [4] while young sediments (lower cretaceous in age) cover the Precambrian basement [32].

3. Material and Method

3.1. Data Collection and Packaging. The measurement of gravity fields can be used to calculate relative and absolute values regarding variations of the fields across earth surface. It is linked to frameworks like Global Positioning System and Digital Terrain Model. The data are treated with respect to the equipment used (for example, Scintrex CG3/CG5 relative gravity meters or Micro-g Lacoste and Romberg as shown in Figure 3).

The data is processed to remove undesirable influences from the surroundings in order to isolate Bouguer anomaly (BA). It represents the difference between the measured and calculated gravity (formula (1)). BA is then modeled to derive geological features for characterizing, quantifying, and interpreting the mass or density distributions in the soil.

$$BA(\varphi,\lambda,h) = g_{mes(\varphi,\lambda,h)} - \left(\gamma_{0(\varphi)} + C_{Free\ air(\varphi,h)} + C_{Bouguer(\varphi,h)_{slab/curvature}} + C_{Terrain(\varphi,\lambda,h)_{topography/bathymetry}}\right), \quad (1)$$

where φ, λ *and* h represent the latitude, longitude, and elevation, respectively, $g_{mes(\varphi,\lambda,h)}$ measures the gravity, $\gamma_{0(\varphi)}$represents the theoretical gravity, $C_{Free\ air(\varphi,h)}$, $C_{Bouguer(\varphi,h)_{slab/curvature}}$, and $C_{Terrain(\varphi,\lambda,h)_{topography/bathymetry}}$ stand,

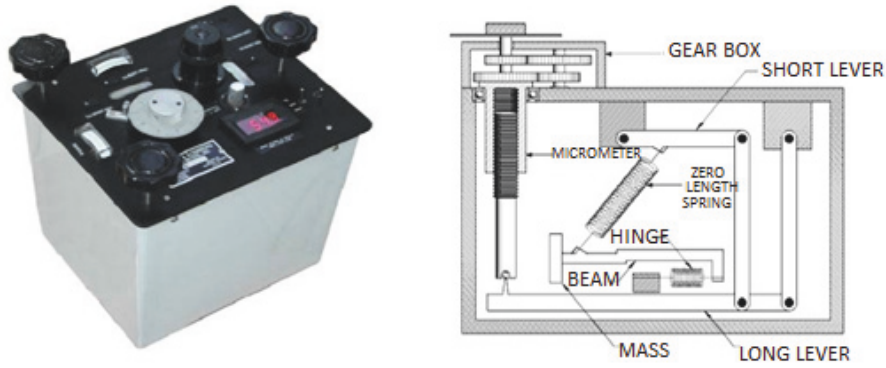

Figure 3: Lacoste and Romberg G/D gravity meters (Micro-g Lacoste, USA).

respectively, for free air, slab/curvature, and topography corrections.

We aim to develop a connectionist model (Neural Network) to correlate Bouguer anomalies with the geographical variables. In general, an array of Artificial Neural Networks is a juxtaposition of unitary, functional, and interconnected elements [33, 34]. There are a multitude of possible arrangements [35]. We choose to use the Multilayer Perceptron (MLP). It is mostly used in time series prediction because of its general property of being universal parsimonious approximator [36]. In its architecture, the neurons are organized in layers as shown in Figure 4.

The inputs x_k, $k=1,\ldots,K$ are multiplied by weights $w^k{}_{ji}$ and summed up together with the constant bias term $\theta^k{}_j$. The resulting n_3^1 is the input to the activation functions g and f. The activation function is originally chosen to be a relay function, but for mathematical convenience a hyperbolic tangent (tanh) or a sigmoid function is most commonly used.

The output y of the MLP network is given by equation below:

$$\begin{aligned} y &= g\left(\sum_{j=1}^{3} w_{ji}^2 g\left(n_j^1\right) + \theta_j^2\right) \\ &= f\left(\sum_{j=1}^{3} w_{ji}^2 g\left(\sum_{k=1}^{K} w_{kj}^1 x_k + \theta_j^1\right) + \theta_j^2\right). \end{aligned} \tag{2}$$

From (2), the MLP network is a nonlinear parameterized map from input space $x \in \mathrm{R}^{\mathrm{K}}$ to output space $\mathrm{y} \in \mathrm{R}^{\mathrm{m}}$ (here m=3). The parameters are the weights $w^k{}_{ji}$ and the biases. f and g are activation functions defined in advance. In our study, we have used tansig for the hidden layer and purelin for output layer. Given input-output data, (x_k, y), 1,..., N, finding the best MLP network is formulated as a data fitting problem. The parameters to be determined are ($w^k{}_{ji}$, $\theta^k{}_j$).

From an arbitrary weight (random value) defined at the beginning, the weights are adjusted by backpropagating the error according to the expression:

$$w_{ji}(n) = w_{ji}(n-1) + \Delta w_{ji}(n), \tag{3}$$

where

$$\Delta w_{ji}(n) = -\eta \frac{\partial E(n)}{\partial w_{ji}(n)} = \eta \delta_j(n)\, y_i(n), \tag{4}$$

where the local gradient δ_j is defined in

$$\delta_j(n) = \begin{cases} e_j(n)\, y_j(n)\left[1 - y_j(n)\right], & \text{if } j \in \text{output layer}, \\ y_j(n)\left[1 - y_j(n)\right] \sum_k \delta_k(n)\, w_{kj}(n), & \text{if } j \in \text{hidden layer}. \end{cases} \tag{5}$$

In (5), e_j is the difference between the output y and target d values, as shown in

$$e_j(n) = d_j(n) - y_j(n). \tag{6}$$

E(n) is the sum of the quadratic errors observed on the set of output neurons written as

$$E(n) = \frac{1}{2} \sum_{j \in C} e_j^2(n). \tag{7}$$

3.2. Shape of MLP. The data set is composed of 2922 samples which comprise latitude, longitude, elevation, and the corresponding Bouguer anomalies. These data are extracted from a database computed for the whole Cameroon by Collignon [37] and Poudjom-Djomani [38]. They cover the study area, the Northern Cameroon, and its surroundings located between longitude of 12° and 16°E and latitude of 8° and 12°N (Figure 5).

60% of these data (1754 samples) are used for training, 20% of the data (584 samples) are used for the validation, and 20% (584 samples) for testing the models. Data conditioning processes are conducted to speed up the training ANNs, which includes interpolating missing data, normalizing the data, and then randomizing them. Usually, the missing data are calculated imprecisely by averaging the neighboring values. In this study, the missing values are forecasted by ANN.

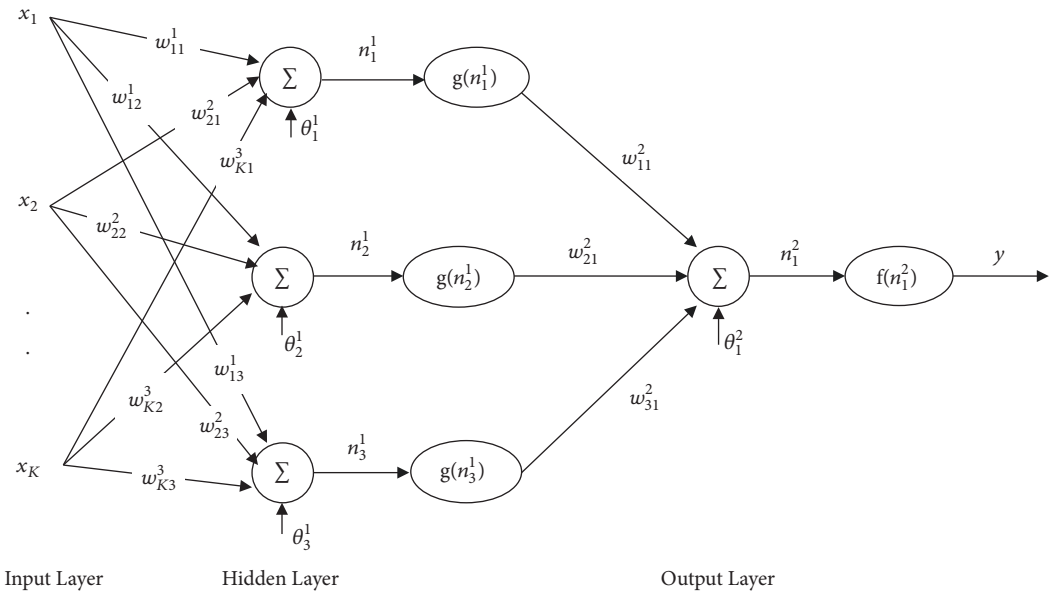

FIGURE 4: Details of a neuron (with $x_1, x_2, \ldots, x_k$ inputs and one output g_j).

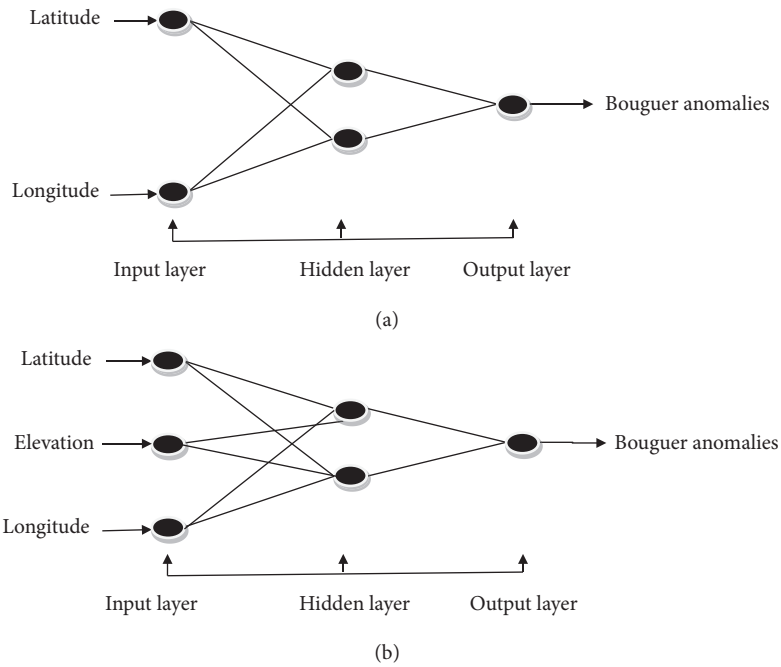

FIGURE 5: Multilayered Perceptron (MLP) network for (a) 2 inputs and (b) 3 inputs.

3.3. Training Algorithm. The diagram (Figure 6) stresses the steps to follow when implementing this scheme of ANN using Levenberg-Marquardt algorithm scheme:

$$w_{k+1} = w_k - \left(J_K^T J_k + \mu I\right)^{-1} J_k e_k, \tag{8}$$

The algorithm adjusts the weights according to (8) where J is the Jacobian, μ is positive and called combination coefficient, I is the identity matrix, and e the error vector. This algorithm takes more memory but less time. Training automatically stops when generalization stop improving, as indicated by an increase in the mean square error of the validation sample.

3.4. Results and Discussion. To quantitatively evaluate the ANN and verify its trend, we conduct statistical analysis involving the coefficient of determination (R^2), the Root Mean Square Error (RMSE), and the Mean Bias Error (MBE). The network structure identification is 2-190-1 and 3-370-1, respectively, for 2 and 3 inputs where the first number indicates number of neurons in the input layer, the last

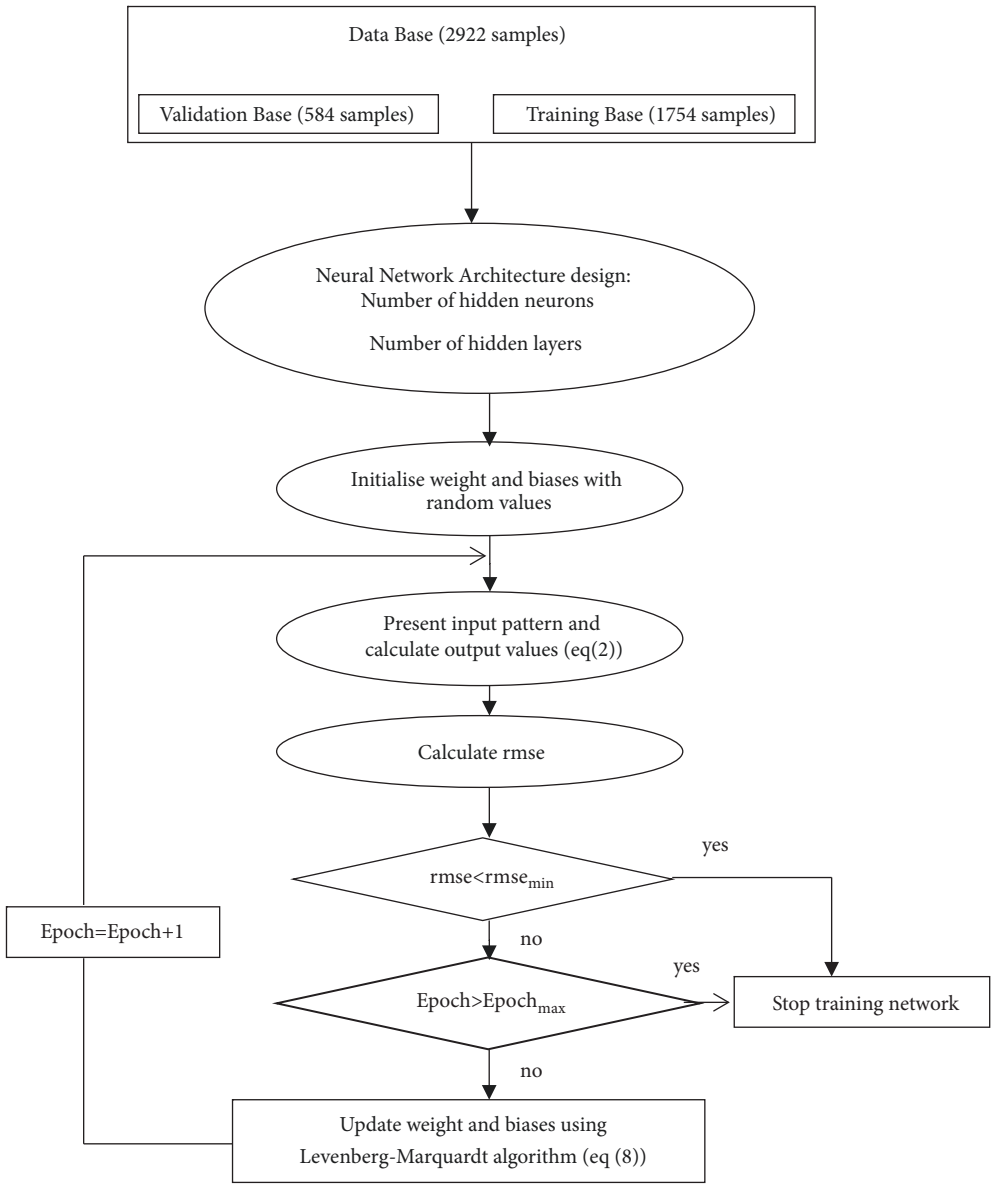

Figure 6: General layout of the neural model.

number represents neurons in the output layer, and the numbers in between represent neurons in the hidden layers. We present the best achieved results for the MLP ANN models (Figures 7 and 8).

As shown in Figures 8 and 9, we observe a good match on the plot for regression for all data in both networks, where R^2 has values of 0.95027 and 0.94254, respectively, for two and three inputs; only a few data are not too close to the fitting line. There is a slight difference between the two models; that with two inputs yields a suitable correlation of 97.48% with less neuron in the hidden layer whereas the model with three inputs yields a 97.08%, coefficient of determination.

MBE and RMSE yield very low values as shown below:

(i) For model 1 (model inputs L and l) the network structure is 2-190-1 for 0.95027, 0.10, and 0.89 representing, respectively, R^2, RMSE and MBE.

(ii) For model 2 (model input L-l-h), the network structure is 3-370-1 and the values of statistical errors R^2, RMSE, and MBE are, respectively, 0.94254, 0.13, and 1.14.

The results indicate that, for the test base, there is a very good correlation (Figures 9 and 10). This signifies the

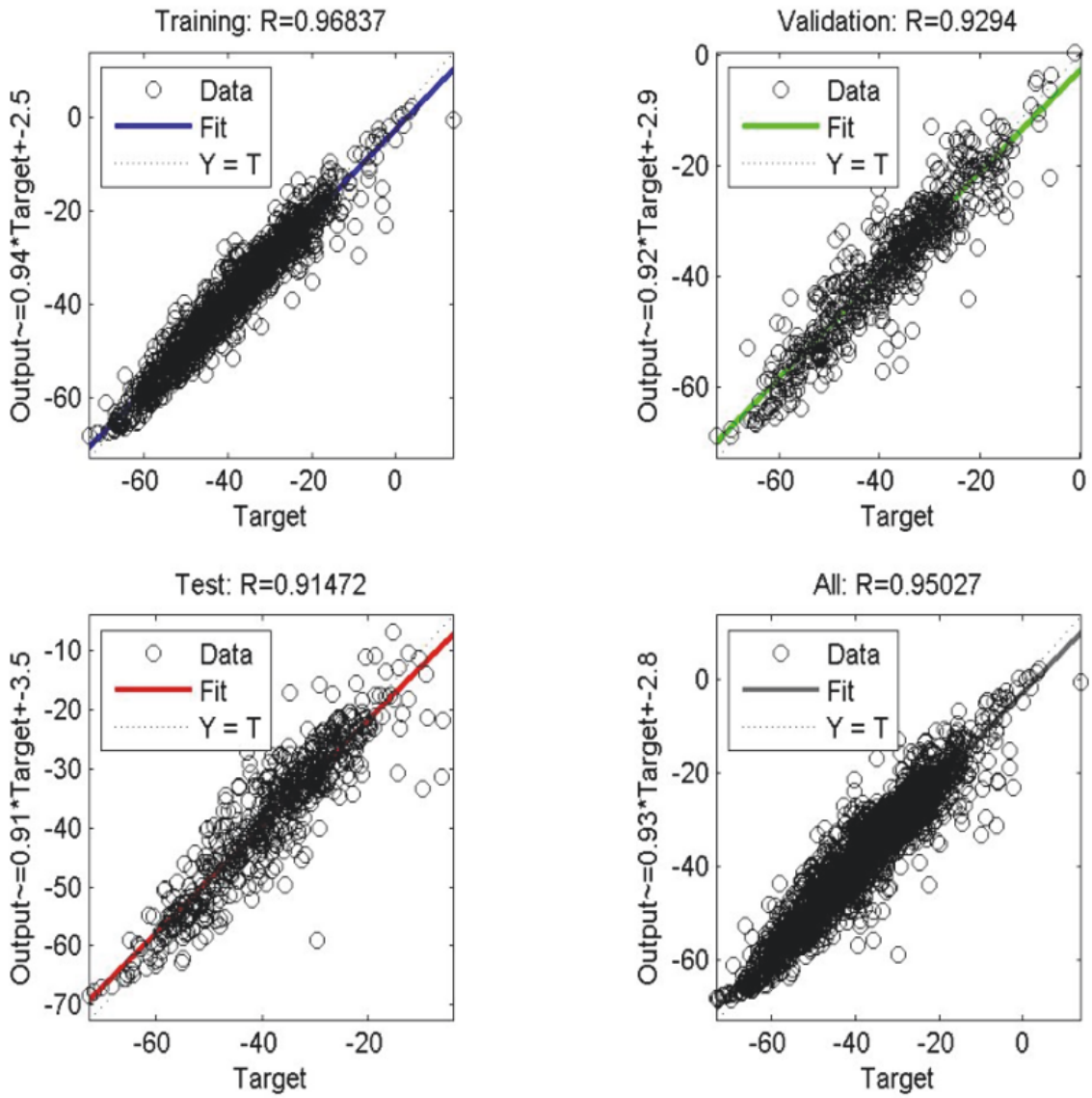

Figure 7: Performance (regression) of ANN model for prediction of Bouguer anomalies around Benue trough with 2 inputs.

possibility of having values of anomalies for areas where they do not exist by giving the geographical location.

Comparing observed and simulated data, we can see as shown in Figures 9 and 10 a good match for two and three entries.

Model Validation. We now compare results obtained using ANNs to classical approaches and, in addition, Bouguer, Euler, and lineaments maps for two and three entries.

Comparing ANNs Results to Other Methods. For two entries, we compare Neural Networks with classical methods based on multiple linear regression with specific approaches developed in most software used in geophysics such as Surfer and Oasis Montaj (Table 1). Z, the anomaly, is given by

$$Z = Ax + By + C, \tag{9}$$

where A, B, and C are constants to be determined; x and y are geographical coordinates of a given point.

For three inputs, we use a classical multiple linear regression implemented through a matrix approach programmed [39] in Matlab or Excel to solve

$$Z = Ax + By + Ch + D, \tag{10}$$

where A, B, C, and D are constants to be determined; x, y, and h, respectively, are geographical coordinates and elevation of a given point.

For Multiple Linear Regression Analysis, the following constants were obtained:

(i) Multiple Linear Regression Analysis with 2 inputs (MLRA2): $A = -1,6229$; $B = 2,7449$; $C = -42,2721$

(ii) Multiple Linear Regression Analysis with 3 inputs (MLRA3): $A = -0,7526$; $B = 1,4844$; $C = -0,0376$; $D = -29,1101$.

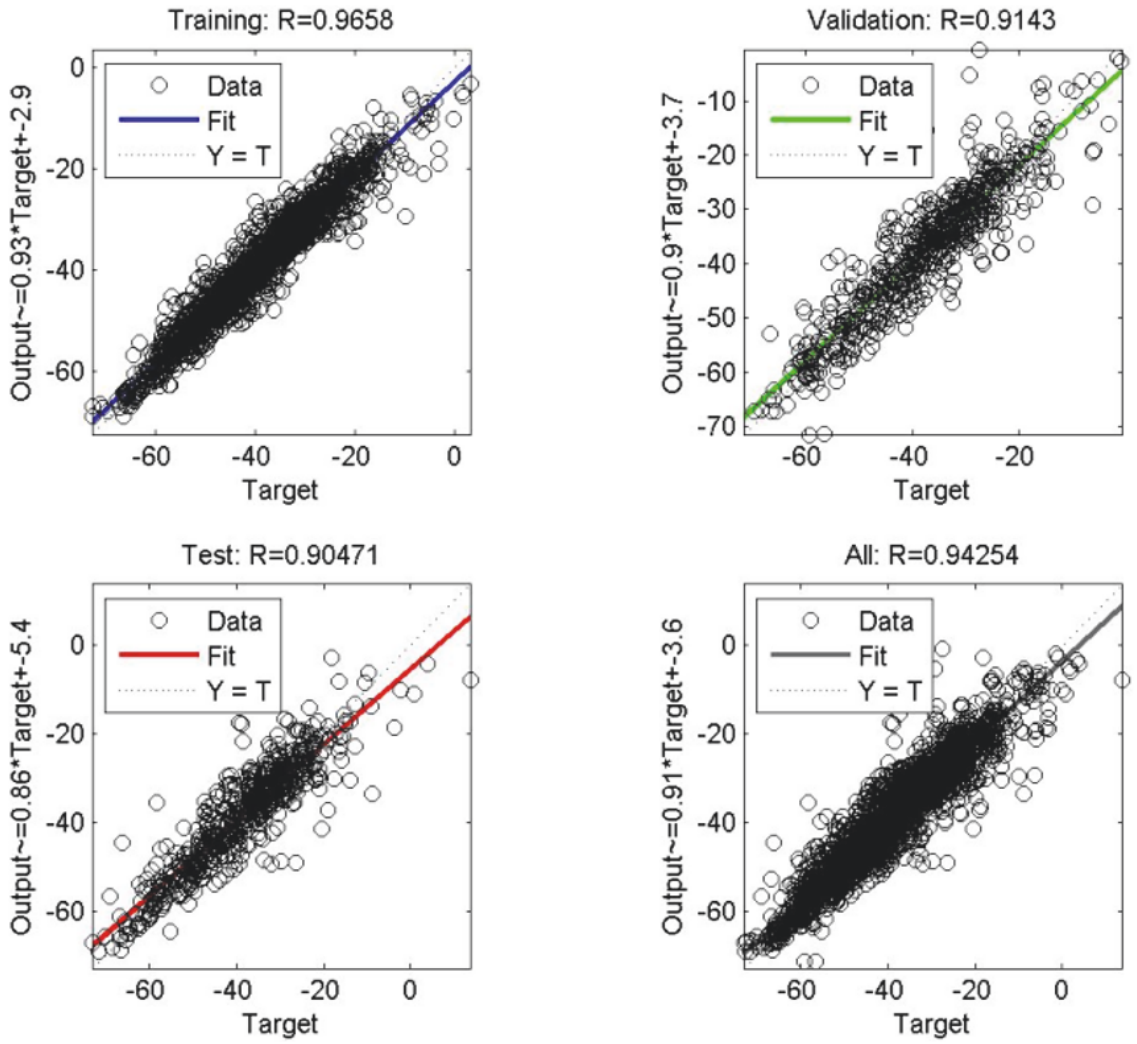

Figure 8: Performance of ANN model for prediction of Bouguer anomalies around Benue trough with 3 inputs.

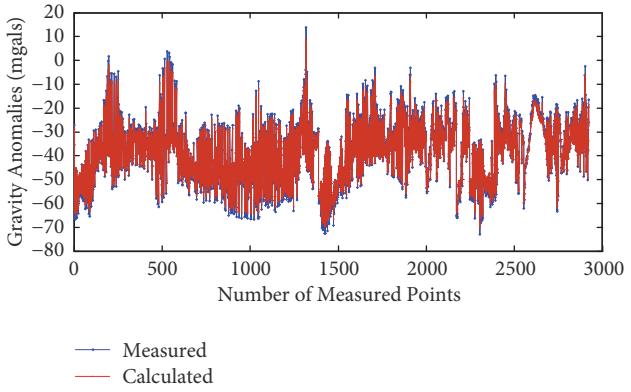

Figure 9: Comparison of present ANN model (blue color) and measured anomalies (red color) for two inputs (y-axis for Bouguer anomalies and x-axis for gravity stations).

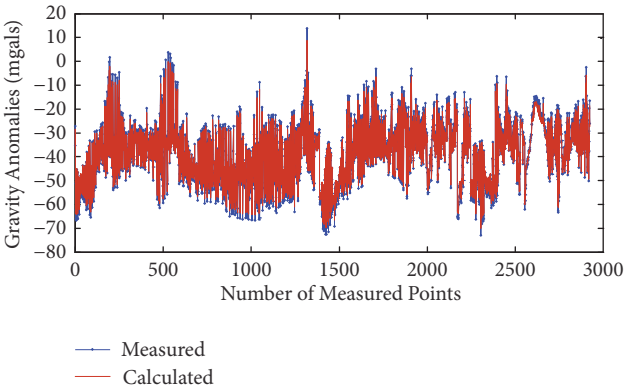

Figure 10: Comparison of present ANN model (blue color) and measured anomalies (red color) for three inputs.

In Figure 11, we represent Bouguer anomalies versus the outputs inferred from MLRA3. In addition, in Table 2 and Figure 12, we analyze the evolution of errors and Root Mean Square Error (RMSE) against the number of iterations and neurons in the hidden layer (NI and NNHL, respectively).

Table 1: Comparing interpolation methods.

Methods	Correlation factor	Mean Bias Error	Root Mean Square Error
	2 inputs		
ANN2	0,95	0,89	0,10
Kriging	0,06114	-0,00142648	12,2701515
Minimum Curvature	0,06114	-0,00142648	12,2701515
Radial Basis Function	0,06114	-0,00142648	12,2701515
Polynomial Regression	0,06099	0,00476981	12,2701501
Multiple linear regression	0,0610	5,2595e-11	12,2680
Inverse distance to a Power	0,06099	0,00476981	12,2701501
	3 inputs		
Multiple linear regression analysis	0,2273	-9,5263e-11	11,1289
ANN3	0,942	1,14	0,13

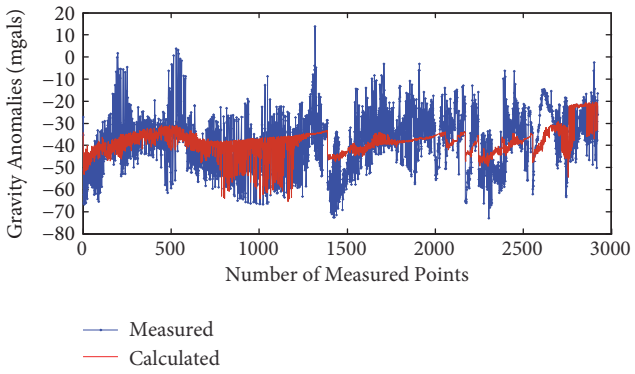

Figure 11: MLRA3 (red color) versus Bouguer anomalies measured (blue color).

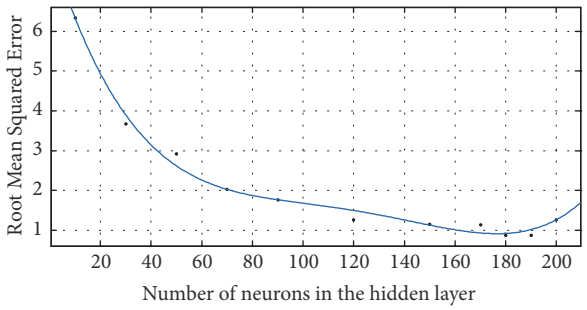

Figure 12: Root Mean Square Error (RMSE) versus number of neurons in the hidden layer (NNHL) for two inputs.

Plotting errors against iterations to us did not have any mathematical explanation; instead we plot errors against number of neurons in the hidden layer where it is obvious that one has low value of RMSE with increasing number of neurons in the hidden layer, unless the situation (above 190) where there is an overfitting (increasing RMSE) exists. The same conclusion arises for three inputs (Figure 13).

The results obtained show very good precision for Neural Network compared to classical approaches. Though ANNs can approximate any function, regardless of its linearity, they have some limitations such as their "black box" nature,

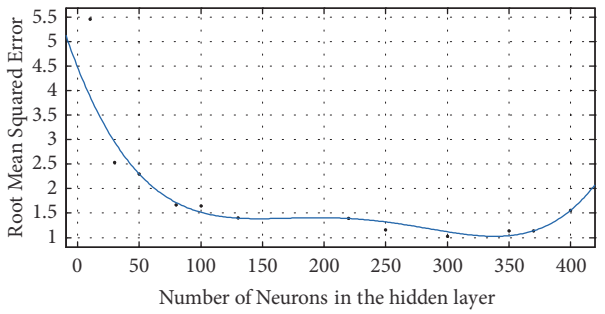

Figure 13: Root Mean Square Error (RMSE) versus number of neurons in the hidden layer (NNHL) for three inputs.

Table 2: Errors against the number of iterations and neurons in the hidden layer for 2 inputs.

Iterations	NN	RMSE	MBE
34	10	6,33	-0,25
97	30	3,68	-0,17
37	50	2,92	0,24
92	70	2,03	0,039
47	90	1,77	0,049
28	120	1,27	0,05
63	150	1,15	-0,165
21	170	1,14	0,13
64	180	0,88	0,0456
36	190	0,88	0,0456
15	200	1,27	-0,15

greater computational burden, increasing accuracy by a few percent which can bump up the scale by several magnitudes (proneness to overfitting), and the empirical nature of model development (needs a lot of data for the training and cases for validation and test).

Comparing Measured and Calculated Bouguer, Euler, and Lineaments Maps. We generate and discuss the data obtained through ANN by establishing Bouguer, Euler (Reid et al.

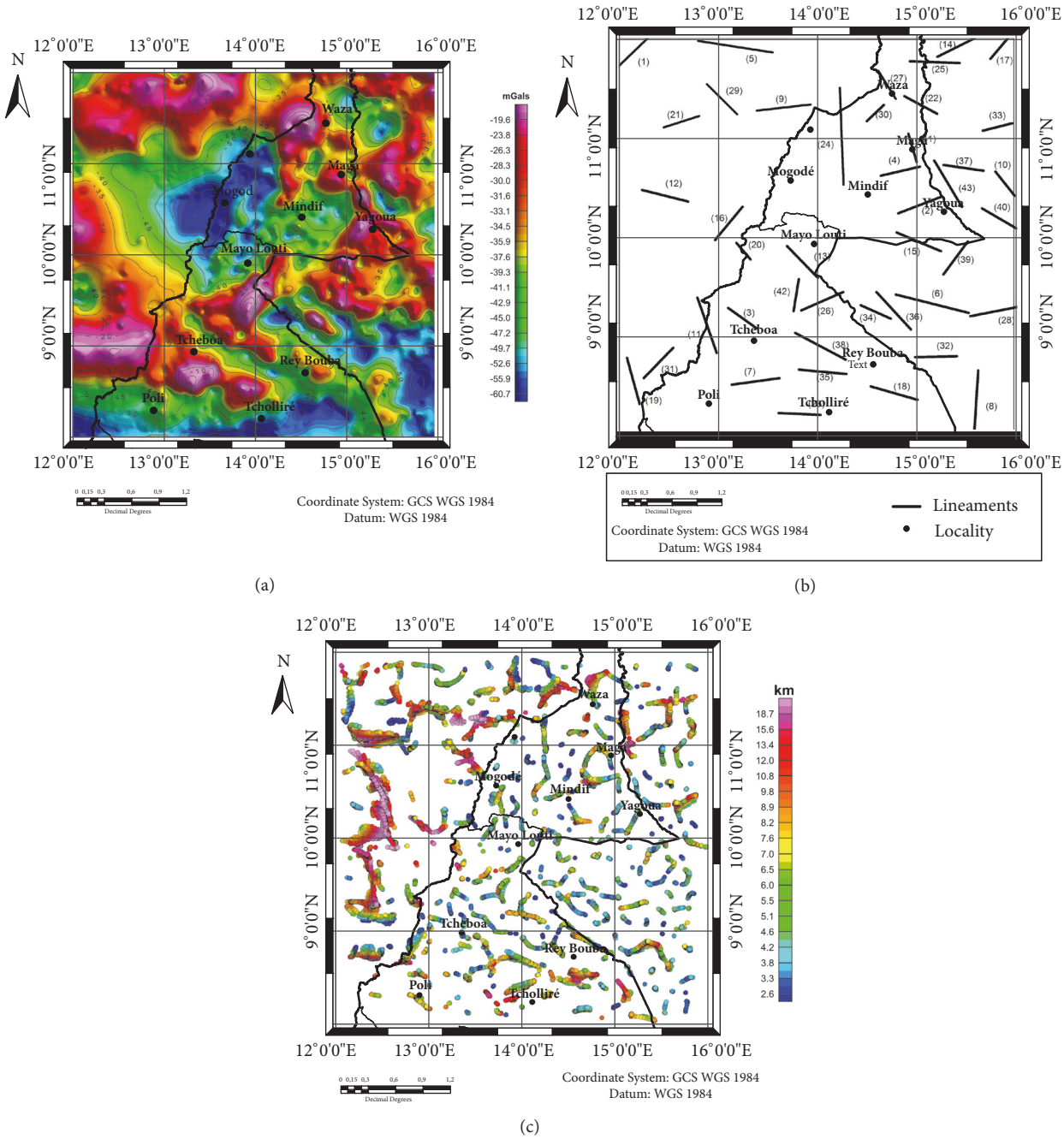

Figure 14: Bouguer (a), lineaments (b), and Euler maps (c).

[40]; (formula (11)), and lineament maps from Bouguer data obtained after prediction through inversion using Oasis Montaj 6.3 software.

$$(x - x_0)\frac{\partial T}{\partial x} + (y - y_0)\frac{\partial T}{\partial y} + (z - z_0)\frac{\partial T}{\partial z} = N(B - T), \tag{11}$$

where T is the total field of magnetic or gravity source detected at (x, y, z), B is the regional gravity or magnetic field, and N is the structural index value that needs to be chosen according to a prior knowledge of the source geometry.

Bouguer, Bouguer 2 and 3 entries maps (Figures 14(a), 15(a), and 16(a)) present structurally the same geological entities. A strict analysis makes it possible to distinguish between these maps: the positive anomaly structures (Waza, Maroua, South of Tcheboa, and Yagoua); the negative anomaly structures (Mogobé, south boundary of the area); and the gradient zones ensuring the transition between these anomalies of different signatures. These different features are the

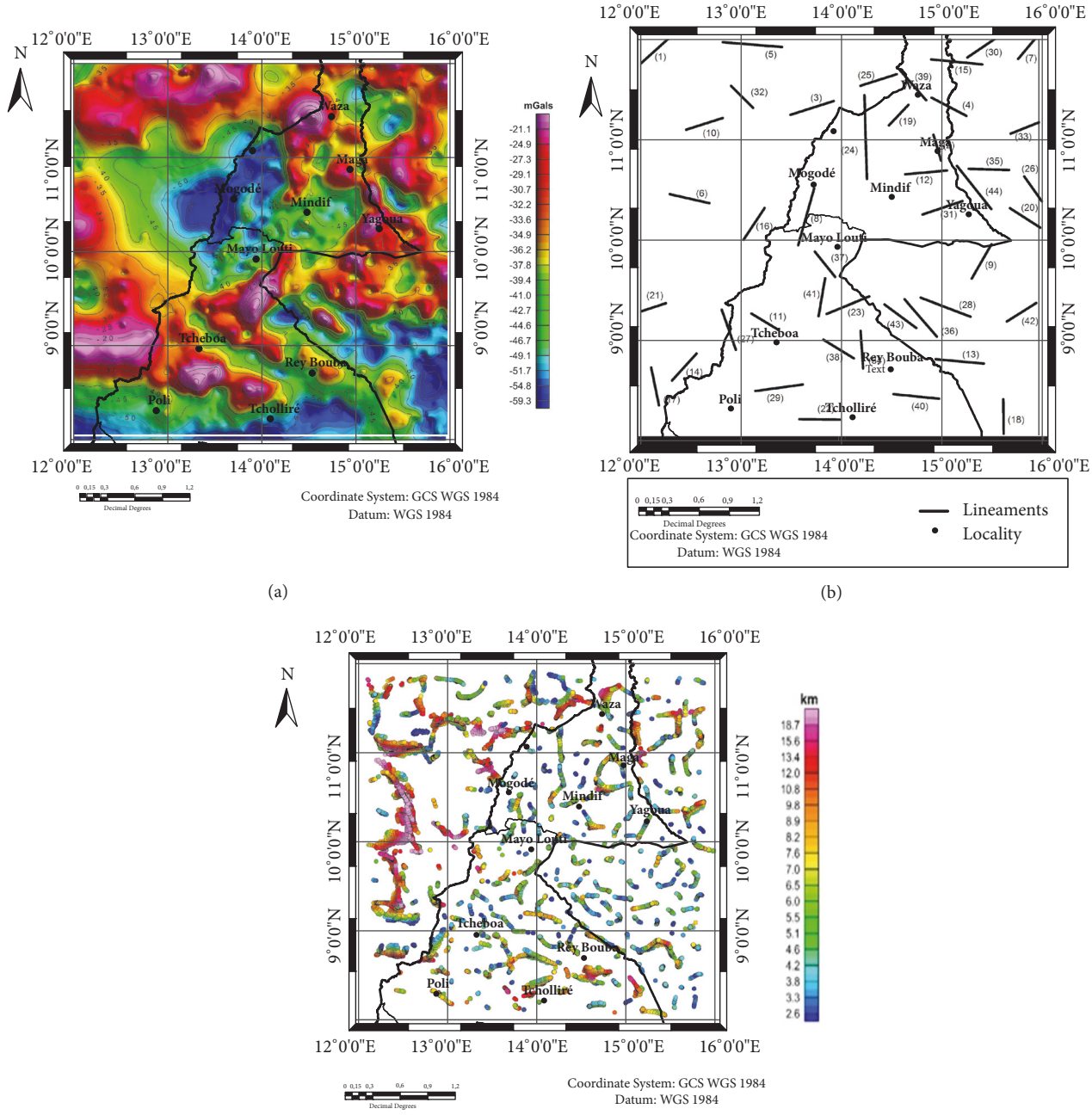

Figure 15: Bouguer (a), lineaments (b), and Euler maps (c) for two entries.

signature of the Precambrian, Early Cretaceous, and Tertiary-Quaternary rocks in the studied area. Transitions between structures require better materialization.

By using and comparing also Bouguer, Bouguer 2 entries, and Bouguer 3 entries, there is also a similarity between the lineament maps (Figures 14(b), 15(b), and 16(b)), thus highlighting tectonics in the area. Between Euler maps (Figures 14(c), 15(c), and 16(c)), the depths of the source structures of anomalies are described.

The lineaments obtained are later compared with existing results from other works. From Figures 14–16, we have a network of faults (above forty) with similar strikes. The depths range from about 2.6 km (at Tcheboa, Garoua sedimentary basin) to about 18.7 km (north of Waza). The results obtained by inversion of gravity data match and complete those obtained by Mouzong et al. [41], Eyike et al. (2010), and Kamguia et al. [4].

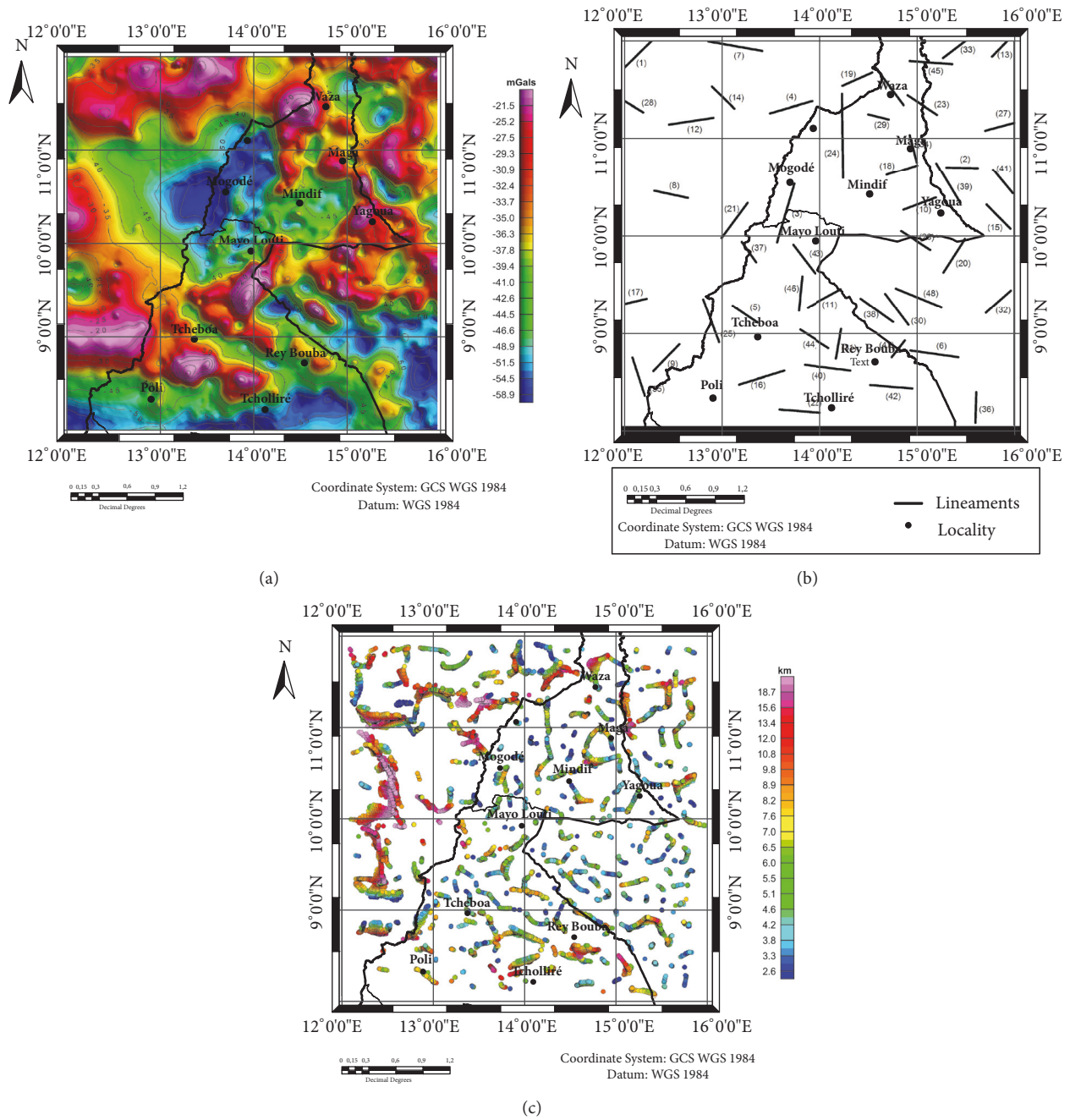

Figure 16: Bouguer (a), lineaments (b), and Euler (c) maps obtained for three inputs.

The ANN based model for gravity anomalies is accurate for the prediction of these anomalies in Northern Cameroon and its surroundings.

4. Conclusion

In this paper, an Artificial Neural Network (ANN) model was estimated for the prediction of gravity anomalies using, respectively, two (longitude and latitude) and three (longitude, latitude, and elevation) inputs in Northern Cameroon and its surroundings along with the corresponding anomaly. Existing gravity data were used for training, validation, and testing of the Neural Network. With each of these inputs, we obtained a good correlation on the plot for regression for all data in both networks, where R^2 has values of 0.95027 and 0.94254, respectively. In order to validate the model, results were compared to those from classical interpolation approaches; in addition Bouguer, Euler, and lineaments maps were compared to our prediction. Low values of MBE and RMSE indicate the effectiveness of the approach. We provide in this work new deep faults for the studied area. The model is promising for evaluating the gravity anomaly at a specific

point where there is no measured value. This method can therefore be recommended in geophysics to improve the resolution of geological features for uneven coverage of recorded gravity data and also to reduce the cost of geophysical surveys.

Data Availability

The data used to support the findings of this study are available from the corresponding author upon request.

Conflicts of Interest

The authors declare that there are no conflicts of interest regarding the publication of this paper.

Acknowledgments

The authors are indebted to IRD (Institut de Recherche pour le Developpement) for providing them with the data used in this work.

References

[1] A. Eyike, F. E. Nyam, and C. A. Basseka, "Topography of the Moho Undulation in Cameroon from Gravity Data: Preliminary Insights into the Origin, the Age and the Structure of the Crust and the Upper Mantle across Cameroon and Adjacent Areas," *Open Journal of Geology*, vol. 08, no. 01, pp. 65–85, 2018.

[2] H. E. Ngatchou, G. Liu, C. T. Tabod et al., "Crustal structure beneath Cameroon from EGM2008," *Geodesy and Geodynamics*, vol. 5, no. 1, pp. 1–10, 2014.

[3] A.-P. K. Tokam, C. T. Tabod, A. A. Nyblade, J. Julià, D. A. Wiens, and M. E. Pasyanos, "Structure of the crust beneath Cameroon, West Africa, from the joint inversion of Rayleigh wave group velocities and receiver functions," *Geophysical Journal International*, vol. 183, no. 2, pp. 1061–1076, 2010.

[4] J. Kamguia, E. Manguelle-Dicoum, C. T. Tabod, and J. M. Tadjou, "Geological models deduced from gravity data in the Garoua basin, Cameroon," *Journal of Geophysics and Engineering*, vol. 2, no. 2, pp. 147–152, 2005.

[5] O. P. N. Eloumala, P. M. Mouzong, and B. Ateba, "Crustal structure and seismogenic zone of cameroon: integrated seismic, geological and geophysical data," *Open Journal of Earthquake Research*, vol. 3, pp. 152–161, 2014.

[6] P. Wessel and W. H. F. Smith, "New version of GMT released," *Transactions of The American Geophysical Union*, vol. 72, no. 441, pp. 445-446, 1995.

[7] W. H. F. Smith and P. Wessel, "Gridding with continuous curvature splines in tension," *Geophysics*, vol. 55, no. 3, pp. 293–305, 1990.

[8] D. G. Krige, *Geostatistics for Oreevaluation*, South African Institute of Mining and Metallurgy, Johannesburg, South Africa, 1978.

[9] N. Cressie, "Spatial prediction and ordinary kriging," *Mathematical Geology*, vol. 20, no. 4, pp. 405–421, 1988.

[10] D. C. Skeels, "What is residual gravity?" *Geophysics*, vol. 32, no. 5, pp. 872–876, 1967.

[11] H. Inoue, "A least-squares smooth fitting for irregularly spaced data: finite-element approach using cubic B-spline basis.," *Geophysics*, vol. 51, no. 11, pp. 2051–2066, 1986.

[12] S. S. Haykin, *Neural Networks and Learning Machines*, MCMaster University, Hamilton, Canada, 3rd edition, 1993.

[13] M. E. Murat and A. J. Rudman, "Automated first arrival picking. A neural network approach," *Geophysical Prospecting*, vol. 40, pp. 587–604, 1992.

[14] M. D. McCormack, D. E. Zaucha, and D. W. Dushek, "First-break refraction event picking and seismic data trace editing using neural networks," *Geophysics*, vol. 58, no. 1, pp. 67–78, 1993.

[15] M. Moustra, M. Avraamides, and C. Christodoulou, "Artificial neural networks for earthquake prediction using time series magnitude data or Seismic Electric Signals," *Expert Systems with Applications*, vol. 38, no. 12, pp. 15032–15039, 2011.

[16] J. Reyes, A. Morales-Esteban, and F. Martínez-Álvarez, "Neural networks to predict earthquakes in Chile," *Applied Soft Computing*, vol. 13, no. 2, pp. 1314–1328, 2013.

[17] M. M. Poulton, B. K. Sternberg, and C. E. Glass, "Location of subsurface targets in geophysical data using neural networks," *Geophysics*, vol. 57, no. 12, pp. 1534–1544, 1992.

[18] Y. Zhang and K. V. Paulson, "Magnetotelluric inversion using regularized Hopfield neural networks," *Geophysical Prospecting*, vol. 45, no. 5, pp. 725–743, 1997.

[19] G. Roth and A. Tarantola, "Neural networks and inversion of seismic data," *Journal of Geophysical Research: Atmospheres*, vol. 99, no. 4, pp. 6753–6768, 1994.

[20] H. Langer, G. Nunnari, and L. Occhipinti, "Estimation of seismic waveform governing parameters with neural networks," *Journal of Geophysical Research: Solid Earth*, vol. 101, no. 9, pp. 20109–20118, 1996.

[21] C. Calderón-Macías, M. K. Sen, and P. L. Stoffa, "Automatic NMO correction and velocity estimation by a feedforward neural network," *Geophysics*, vol. 63, no. 5, pp. 1696–1707, 1998.

[22] H. Dai and C. MacBeth, "Split shear-wave analysis using an artificial neural network?" in *First Break*, vol. 12, pp. 605–613, 1994.

[23] Z. Huang, J. Shimeld, M. Williamson, and J. Katsube, "Permeability prediction with artificial neural network modeling in the Ventura gas field, offshore eastern Canada," *Geophysics*, vol. 61, pp. 422–436, 1996.

[24] L.-X. Wang and J. M. Mendel, "Adaptive minimum prediction-error deconvolution and source wavelet estimation using Hopfield neural networks," *Geophysics*, vol. 57, no. 5, pp. 670–679, 1992.

[25] C. Calderón-Macías, M. K. Sen, and P. L. Stoffa, "Hopfield neural networks, and mean field annealing for seismic deconvolution and multiple attenuation," *Geophysics*, vol. 62, no. 3, pp. 992–1002, 1997.

[26] F. U. Dowla, S. R. Taylor, and R. W. Anderson, "Seismic discrimination with artificial neural networks: Preliminary results with regional spectral data," *Bulletin of the Seismological Society of America*, vol. 80, pp. 1346–1373, 1990.

[27] G. Romeo, "Seismic signals detection and classification using artificial neural networks," *Annals of Geophysics*, vol. 37, pp. 343–353, 1994.

[28] A. A. Grêt, E. E. Klingelé, and H.-G. Kahle, "Application of artificial neural networks for gravity interpretation in two dimensions: A test study," *Bollettino di Geofisica Teorica e Applicata*, vol. 41, no. 1, pp. 1–20, 2000.

[29] M. Ghalambaz, A. R. Noghrehabadi, M. A. Behrang, E. Assareh, A. Ghanbarzadeh, and N. Heayat, "A hybrid neural network and gravitational search algorithm (HNNGSA) method to solve well known Wessinger's equation," *International Journal*

of Mechanical, Aerospace, Industrial, Mechatronic and Manufacturing Engineering, vol. 5, no. 1, pp. 147–151, 2011.

[30] J. D. Fairhead and C. S. Okereke, "A regional gravity study of the West African rift system in Nigeria and Cameroon and its tectonic interpretation," *Tectonophysics*, vol. 143, no. 1-3, pp. 141–159, 1987.

[31] I. Ngounouno, B. Déruelle, and D. Demaiffe, "Petrology of the bimodal Cenozoic volcanism of the Kapsiki plateau (northernmost Cameroon, Central Africa)," *Journal of Volcanology and Geothermal Research*, vol. 102, no. 1-2, pp. 21–44, 2000.

[32] J.-C. Dumort and Y. Péronne, *Carte Géologique de Reconnaissance à l'échelle du 1/500000, République Féderale du Cameroun, feuille Maroua*, avec notice explicative, BRGM et Direction des Mines et de la Géologie, Kribi, Cameroun, 1966.

[33] S. Bofinger and G. Heilscher, "Solar electricity forecast-approaches and first results," in *Proceedings of the in. 21th PV Conference*, Dresden, Germany, 2006.

[34] A. Bosch, A. Miñán, C. Vescina et al., "Fourier Transform Infrared Spectroscopy for rapid identification of nonfermenting gram-negative bacteria isolated from sputum samples from cystic fibrosis patients," *Journal of Clinical Microbiology*, vol. 46, no. 12, pp. 2535–2546, 2008.

[35] J. F. Jodouin, *Les réseaux de neurones: principes et définitions*, Hermès, Paris, France, 1994.

[36] K. Hornik, "Approximation capabilities of multilayer feedforward networks," *Neural Networks*, vol. 4, no. 2, pp. 251–257, 1991.

[37] F. Collignon, *Gravimétrie de reconnaissance de la République Fédérale du Cameroun*, ORSTOM, Paris, France, 1968.

[38] Y. H. Poudjom-Djomani, *Apport de la gravimétrie à l'étude de la lithosphère continentale et implications géodynamiques. Etude d'un bombement intraplaque: le massif de l'Adamaoua (Cameroun) [Thèse de Doctorat]*, Université de Paris-Sud, Orsay, France, 1993.

[39] H. B. Scott, "Multiple Linear Regression Analysis: a matrix approach in MATLAB," *Alabama Journal of Mathematics, Spring/Fall2009*, 3 pages, 2009.

[40] A. B. Reid, J. M. Allsop, H. Granser, A. J. Millett, and I. W. Somerton, "Magnetic interpretation in three dimensions using Euler deconvolution," *Geophysics*, vol. 55, no. 1, pp. 80–91, 1990.

[41] M. P. Mouzong, J. Kamguia, S. Nguiya, Y. Shandini, and E. Manguelle-Dicoum, "Geometrical and structural characterization of Garoua sedimentary basin , Benue Trough, North Cameroon, using gravity data," *Journal of Biology and Earth Sciences*, vol. 4, no. 1, pp. E25–E33, 2014.